SIViP (2010) 4:247–262
DOI 10.1007/s11760-009-0115-6

ORIGINAL PAPER

Color contrast enhancement method using steerable pyramid transform

D. Cherifi · A. Beghdadi · A. H. Belbachir

Received: 16 September 2008 / Revised: 17 December 2008 / Accepted: 16 March 2009 / Published online: 24 April 2009

Abstract A new method of contrast enhancement based on steerable pyramid transform is presented in this work. The use of steerable filters is motivated by the fact that the images are to be observed by human and therefore it would be better to incorporate some knowledge on the Human Visual System in the design of the image processing tool. Here, the frequency and directional selectivity of the HVS is modeled by the steerable filters. The contrast is amplified using a selective nonlinear function which simulates the nonlinearity response of the HVS to the luminance stimuli. So the basic idea is to enhance the luminance signal irrespective of the two chrominance components using a multidirectional and multiscale decorrelation color transform. Initially the rgb (red, green and blue) color image is converted to lab (luminance and chrominance) color image. Only the luminance component is transformed by the steerable pyramid transform, so that the luminance component is independently decomposed into different scale and orientation sub-bands. The contrast in each sub-band is enhanced using a nonlinear mapping function. Finally the rgb color image is obtained from the enhanced luminance component along with the original chrominance components. The performance of the proposed method is objectively evaluated using spectrum energy analysis and a visibility map based on a perceptual filtering model. The obtained results confirm the efficiency of the method in enhancing subtle details without affecting color balance and without the usual noise amplification and edge ringing effect.

Keywords Angular energy spectrum · Contrast enhancement image and Just-Noticeable Contrast · Multiscale · Multi-orientation · Pyramid representation · Radial energy spectrum · Steerable filters · Visibility map

D. Cherifi · A. H. Belbachir
LAAR, Département Physique, Faculté des Sciences,
Université des Sciences et de la Technologie Mohamed Boudiaf,
BP 1505, El M'Nouar, Oran 31036, Algeria

A. H. Belbachir
e-mail: ahbelbachir@univ-usto.dz

D. Cherifi (✉) · A. Beghdadi
L2TI, Institut Galilée, Université Paris 13, 99 av J. B. Clément,
93430 Villetaneuse, France
e-mail: cherifi@galilee.univ-paris13.fr

A. Beghdadi
e-mail: azeddine.beghdadi@univ-paris13.fr

1 Introduction

Due to the limitations of image acquisition systems image enhancement is of great importance in many applications. Noise filtering, deblurring, coding artifact reduction, luminance adjustment and contrast enhancement are among the most explored field of research in the image processing community. Another interesting issue concerns distortion-free image contrast enhancement. Indeed, any image contrast enhancement tends to produce some artifacts such as edge overshooting, noise amplification, color distortion and ringing effects. Most of the existing image enhancement methods are applied to gray-level images. However, with the evolution of photography, digital color imaging becomes of great interest. The contrast enhancement for color image is consequently in high demand to cope with this advancement [1]. It is naturally believed that the color imaging is nothing but a channel-by-channel intensity-image processing. However, many problems arise when adopting this approach. Indeed, each color channel is not actually orthogonal to the others and luminance and chrominance cannot be easily separated. So a channel-by-channel based processing will frequently result in false colors due to unbalanced equalization between channels. Some efforts have been carried out to solve these problems. One solution is to perform an adaptive neighborhood histogram equalization as proposed by Buzuloiu et al. [2]. Another approach suggested by Trahanias et al. [3] is to perform a 3D histogram equalization method in the RGB cube. Other interesting histogram-based color enhancement methods have been proposed in the literature [4,5]. In Pitas and Kiniklis method [4], the histogram equalization is performed only on luminance and saturation channels. However, it has been reported that the modification of the saturation channel may result in unnatural output images [2]. Niblack [5] has performed histogram equalization directly on the rgb color space and naturally the result does not maintain good color fidelity as discussed above. To overcome this problem Dash and Chatterji [6] proposed an adaptive local contrast enhancement technique which is controlled by some parameters called contrast power and contextual region size. The extension of this method was also proposed by Chartterji and Murthy [7] for color image using rgb color space. All these works confirms that the color space choice is one of the fundamental issues in color image enhancement. Compared with classical colorimetric RGB color space, there are many other "perceptual" color spaces such as HSV (Hue, Saturation, and Value) or HIS (Hue, Intensity and Saturation). However, when any of these components is enhanced alone, color degradation may result such as in the method proposed by Strickland et al. [8]. Similar effects appear when using Gupta and Chanda method [9] which focuses only on hue channel. Naik et al. showed in [10] that the hue components have been preserved without gamut problem. However, all these contrast enhancements generally lead to color distortion. These strengths and limitations are mainly due to the fact that the color spaces used are not adapted to contrast enhancement. Other perceptually uniform color spaces have been considered in the literature. Among these color spaces, CIELAB is believed to be a better approximation of the HVS perception (i.e. HVS is more sensitive to luminance signal rather than the chrominance signal). It allows a simple implementation of contrast enhancement since the color image can be efficiently decomposed into luminance and chrominance. Thus a brightness adjustment to luminance-only or color balancing to chrominance-only could be more feasible. Usually the classical approaches such as histogram equalization or unsharpening do not incorporate the multiscale and directional selectivity. It was found that the introduction of multiscale analysis in the design of image enhancement method yields good results [11,12]. An HVS-based color image enhancement using multiscale analysis has been developed by Huang et al. [13]. Xianghong et al. [14] also proposed another multiscale method for color medical image application. A wavelet-based method using some characteristics of the HVS has been proposed by Xiao and Ohya [15]. All these methods share two points on common, that is, a multi-resolution transform and a color space transform. Then contrast enhancement is applied at different resolutions in the alternative color spaces instead of their initial RGB space. The enhanced color image is then recomposed by the inverse transformation of those enhanced coefficients. However, some drawbacks of wavelet transform have been mentioned such as the lack of rotation and the translation and the orientation.

Another aspect which could be taken into account is the directional selectivity in the image analysis. It was found that when using multiscale and multiorientation analysis better results could be obtained for contrast enhancement [16]. Another difficulty when dealing with image enhancement is the subjective nature of the image quality assessment. At present time there is no satisfying objective image quality assessment. While many image quality metrics have been developed for image distortion estimation [17], there are only a few ad hoc objective measures for image enhancement evaluation [18].

Beyond these approaches, there is still widespread interest to HVS-inspired contrast enhancement methods. Indeed, since the publication of the first version of Retinex theory by Land [19], a number of HVS-based methods have been proposed for the purpose of designing color image enhancement methods. Some approaches based on retinex theory, such as the Single Scale Retinex (SSR) method [20], have been proposed. The idea has been further developed and improved by Meylan and Süsstrunk [21] and later by Choi et al. [22] by introducing in the SSR scheme an adaptive filtering process. However, despite these efforts some undesirable effect may result in the enhanced image limiting thus the efficiency of these methods. Multi-Scale Retinex (MSR) have been developed to solve these problems [23]. However, both SSR and MSR suffer from the graying-out effect which may appear in large uniform color areas in the image. Multi-scale Retinex Color Restoration (MSRCR) has been then introduced [24]. It tends to overcome some of these shortcomings by adopting a multi-scale approach and adaptive restoration posttreatment. However, these drawbacks still remains unsolved as recently reported in [25,26]. Another common drawback of these center/surround methods is that the results depends greatly on the size of the filter. Indeed, a small filter may produce halo and ringing artefacts and a large filter could not enhance subtle details. We believe that the limitation of retinex-based method is also mainly due to the use of the simple and restricted multiplicative model and the estimation of illumination and reflectance.

These drawbacks have been recently discussed by Meyland et al. [26]. It has been shown that by taking into account retinal local nonlinear adaptation some improvements for contrast enhancement could be obtained. However, the aim of their method was only to achieve pleasing reproductions of images and the authors did not give any objective performance evaluation. Despite these efforts, color shift and over-enhancement are still drawbacks of many color image enhancement methods. Furthermore, many of the existing methods do not take into account the directional selectivity of the HSV. Here, we adapt the method developed in [27] to color contrast enhancement. We use the steerable pyramid transform in order to decompose only the luminance component into different scales and directional frequency subbands. Only the medium frequency components are enhanced with a nonlinear mapping function to avoid increasing the noise in low and high frequency bands.

The proposed method is compared with some classical and state-of-art methods. Here, we consider histogram equalization [28], Contrast-Limited Adaptive Histogram Equalization CLAHE [29], Edge-based Local Contrast Enhancement ELCE [30] and unsharpening as classical techniques [31]. We also compare our approaches with the curvelet-based contrast enhancement method [32] and MSRCR method [24]. In order to evaluate the performance of our method, we use both subjective and objective evaluation. The obtained results are evaluated in terms of visual contrast enhancement, color appearance and energy distribution. A new objective evaluation based on Fourier transform is used. Following the idea introduced in [33], the radial and angular energy spectrum at different scales and orientations of the pyramid are computed before and after enhancement. To visualize the enhancement result, a visibility map is extracted from both the original and enhanced luminance component using a perceptual filter model [34]. This map decomposes the luminance component into two classes (visible class and non-visible class).

The paper is organized as follows. The following section introduces briefly the steerable filters and the associated pyramid decomposition. Section 3 describes the method. The next section is devoted to the performance evaluation of the method using an objective and subjective criteria. The results are then discussed in Sect. 5. Finally, we conclude this work and propose some perspectives.

2 Steerable pyramid transform

The Steerable Pyramid Transform SPT was introduced by Freeman and Adelson as an alternative to wavelet transform [35,36]. It permits to decompose an image into noncorrelated components facilitating thus their analysis and processing. It has been shown that SPT overcomes some drawbacks of discrete wavelet transform DWT. Indeed, the SPT is a multiscale and multidirectional representation that is translation-invariant. Furthermore, this representation could be designed in order to make it rotation-invariant. It could be also noticed that SPT has some advantages of orthonormal wavelet transform (e.g. basis function are localized in space and spatial-frequency, the transform is a tight frame) but suffers less from its drawbacks, such as aliasing effects. Another interesting property of the SPT is its polar-separability which is well defined in the Fourier domain. Unlike the DWT, the SPT is overcomplete by the factor $4k/3$. Therefore it is more adapted to image analysis and processing than to image compression. This elegant transformation has been applied in many applications and especially for image quality enhancement [16,27,37].

2.1 Steerable filters

Steerable filters, introduced by Freeman and Adelson [35], are spatial oriented filters that have received a great interest in image analysis. The basic idea is to generate a rotated filter from a linear combination of a fixed set of basis filters [38]. The steerability condition is not restricted to derivative filters and could be expressed for any signal f as:

$$f^{\theta}(x, y) = \sum_{m=1}^{M} k_m(\theta) f^{\theta_m}(x, y) \tag{1}$$

where $f^{\theta}(x, y)$ is the rotated version of f by a arbitrary angle θ, $k_m(\theta)$ are the interpolation functions, $f^{\theta_m}(x, y)$ are the basis functions and M the number of basis functions required to steer the function $f(x, y)$.

To determine the conditions under which a given function satisfies the steering condition in Eq. (1), let us work in polar coordinates ($r = \sqrt{x^2 + y^2}$ and $\phi = \arg(x, y)$). The function f could be expressed as Fourier series in polar angle, ϕ:

$$f(r, \phi) = \sum_{n=-N}^{N} a_n(r) \mathrm{e}^{jn\phi} \tag{2}$$

where $j = \sqrt{-1}$ and N is the discrete length of coefficients.

It has been demonstrate in [37,38] that the steering condition in Eq. (1), is satisfied for functions expandable in the form of Eq. (2) if and only if the interpolation function $k_m(\theta)$ are solution of:

$$c_n(\theta) = \sum_{m=1}^{M} k_m(\theta)(c_n(\theta))^m \tag{3}$$

where $c_n(\theta) = \mathrm{e}^{jn\theta}$, and $n = \{0, \ldots, N\}$.

From Eq. (3), $f^{\theta}(r, \phi)$ is expressed as:

$$f^{\theta}(r, \phi) = \sum_{m=1}^{M} k_m(\theta) g_m(r, \phi) \tag{4}$$

where $g_m(r, \phi)$ can be any set of functions.

It has been also demonstrated that the minimum number M of basis functions required to steer $f(r, \phi)$ is equal to the number of non-zero Fourier coefficients $a_n(r)$.

Fig. 1 The block diagram of the steerable pyramid transform

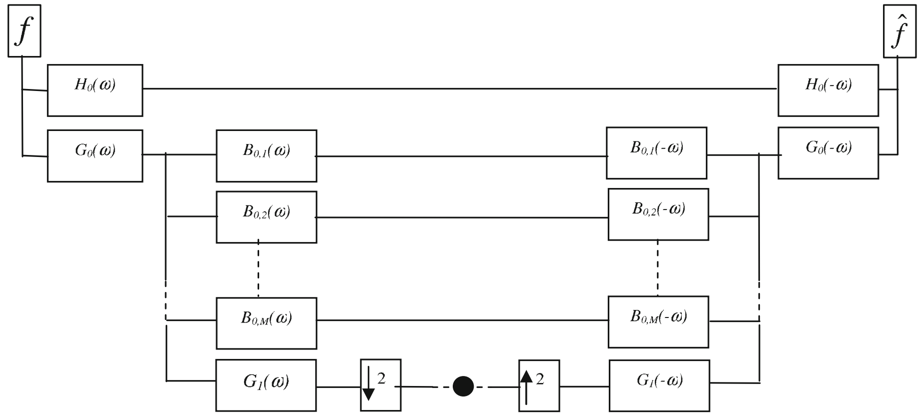

2.2 The steerable pyramid decomposition

Like the discrete wavelet transform, the SPT decomposes an image into a set of scaled and oriented sub-bands. Figure 1 shows a diagram of the SPT with three levels of decomposition and three orientations.

Where f and $\widehat{f}$ are the original and the reconstructed images. H_0, G_0, $B_{k,m}$ and G_1 are the high-pass, the first low-pass, the directional band-pass filters and the second low-pass filter, respectively. It has been show by Karasaridis and Simoncelli [37] that the reconstructed signal in the frequency domain is given by:

$$\widehat{F}(\omega) = \left\{ |H_0(\omega)|^2 + |G_0(\omega)|^2 \times \left[|G_1(\omega)|^2 + \sum_{m=1}^{M} |B_{1,m}(\omega)|^2 \right] \right\} \cdot F(\omega) + a.t \tag{5}$$

where $a.t$ refers to the aliasing terms and $\omega = \sqrt{\omega_x^2 + \omega_y^2}$ is the radial frequency and ω_x and ω_y are the spatial frequencies. It has been shown in [37] that for a perfect reconstruction the three following constraints should be taken into account.

(1) Aliasing effect elimination

$$G_1(\omega) = 0, \quad \text{for} \quad |\omega| > \pi/2 \tag{6}$$

(2) The recursive stability constraint

$$|G_1(\omega/2)|^2 \left[|G_1(\omega)|^2 + \sum_{m=1}^{M} |B_{1,m}(\omega)|^2 \right] = |G_1(\omega/2)|^2 \tag{7}$$

For level k the directional band-pass filters and the low-pass filter are given by:

$$\begin{cases} B_{k,m}(\omega) = B_{k-1,m}(\omega/2) \quad \text{where} \quad m = \{1, \ldots, M\} \\ G_k(\omega) = G_{k-1}(\omega/2) \end{cases} \tag{8}$$

(3) Unity system response amplitude

$$|H_0(\omega)|^2 + |G_0(\omega)|^2 \times \left[|G_1(\omega)|^2 + \sum_{m=1}^{M} |B_{1,m}(\omega)|^2 \right] = 1 \tag{9}$$

Following the notations in [16], the frequency responses of these filters in polar coordinates are given by the following Eqs. (10) to (14).

– The high-pass filter

$$H_0(\omega) = \begin{cases} 0 & \omega < \omega_1 \\ \sqrt{\frac{1}{2}\left[1 - \cos\left(\pi \cdot \frac{\omega - \omega_1}{\omega_{\max} - \omega_1}\right)\right]} & \omega_1 \le \omega \le \omega_{\max} \\ 1 & \omega > \omega_{\max} \end{cases} \tag{10}$$

– The first low-pass filter

$$G_0(\omega) = \begin{cases} 1 & \omega < \omega_1 \\ \sqrt{\frac{1}{2}\left[1 + \cos\left(\pi \cdot \frac{\omega - \omega_1}{\omega_{\max} - \omega_1}\right)\right]} & \omega_1 \le \omega \le \omega_{\max} \\ 0 & \omega > \omega_{\max} \end{cases} \tag{11}$$

where $\omega_{\max}$ is the maximum radial frequency and ω_1 is the frequency at which $G_0(\omega)$ starts to attenuate.

– The second low-pass filter

$$G_1(\omega) = \begin{cases} 1 & \omega < \omega_0 \\ \sqrt{\frac{1}{2}\left[1 + \cos\left(\pi \cdot \frac{\omega-\omega_0}{\omega_1-\omega_0}\right)\right]} & \omega_0 \le \omega \le \omega_1 \\ 0 & \omega > \omega_1 \end{cases} \tag{12}$$

where ω_0 is the frequency at which $G_1(\omega)$ starts to attenuate.

– The non-oriented band-pass filter is given by:

$$B(\omega) = \begin{cases} 1 & \omega < \omega_0 \\ \sqrt{\frac{1}{2}\left[1 - \cos\left(\pi \cdot \frac{\omega-\omega_0}{\omega_1-\omega_0}\right)\right]} & \omega_0 \le \omega \le \omega_1 \\ 0 & \omega_1 \le \omega \le \omega_{max} \end{cases} \tag{13}$$

Following the steerability property, the oriented band-pass filters in m directions are derived as follows:

$$B_m(\omega) = B(\omega)\left(cos(\theta - \theta_m)\right)^M \tag{14}$$

Where $\theta_m = m\pi/(M+1)$ for $m \in \{1, \ldots, M\}$, M is the number of orientations and $\theta = \tan^{-1}(\omega_y/\omega_x)$ is the angular variable in polar coordinates. The frequency responses of the filters used in the decomposition are shown in Fig. 2.

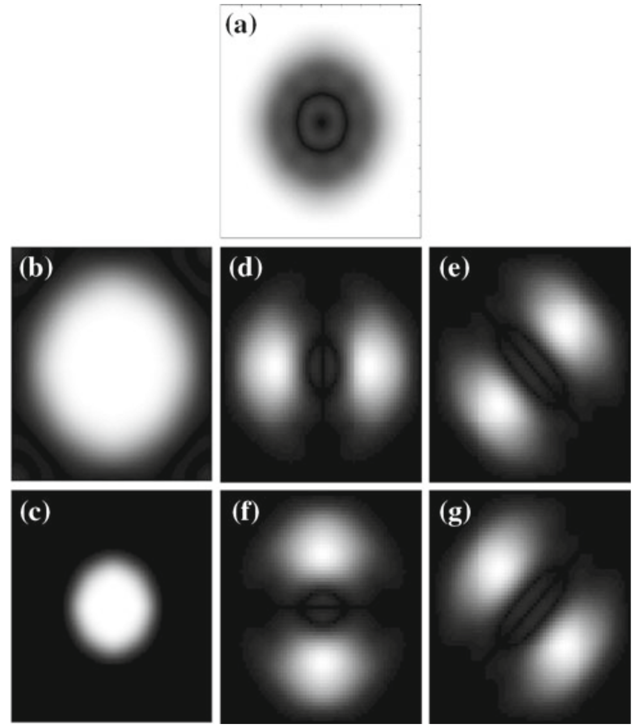

Fig. 2 Frequency responses of the filters. **a** High-pass filter, H_0; **b** first low-pass filter, G_0; **c** second low-pass filter, G_1; **d** band-pass filter 0°, $B_{0,1}$; **e** band-pass filter 45°, $B_{0,2}$; f band-pass filter 90°, $B_{0,3}$; **g** band-pass filter 135°, $B_{0,4}$

3 Contrast enhancement for color image

Multiscale and multidirectional SPT are applied in the proposed method for color image enhancement. Image features at different resolution and orientations are extracted from these pyramidal representation. Then an adaptive non-linear mapping function is applied to these subbands in order to enhance the signal at different resolution and orientations. These transformed components are combined with the other sub-bands and used in the reconstruction step of the final image.

The proposed steerable contrast enhancement method is summarized in Fig. 3 for three levels ($k = \{0, 1, 2\}$) and four orientations ($m = \{1, 2, 3, 4\}$). As can be seen from the figure, the original rgb image is converted to Lab color space with L being the luminance and $a - b$ the corresponding red-green and blue-yellow channels, respectively. Be noted that only luminance channel information is processed here. The extracted luminance information is then decomposed into high-pass and low-pass components (L_h, L_0, respectively). This low-pass component L_0 is then decomposed into M oriented sub-bands $L_{0,1}, L_{0,2}, \ldots, L_{0,M}$ and a lower-pass band L_1. The pyramid is constructed by recursively repeating the operation shown in the dashed box at the dark node. Note that only L_1 is sub-sampled producing reduced images as in the classical pyramid decomposition of Burt and Adelson [39]. The enhanced image can be reconstructed by reversing the process of decomposition. The last lower pass-band is up-sampled at each level of the reconstruction then it is added to all oriented and enhanced band-pass components, $L_{k,m}$ which are mapped by the nonlinear function $T(x)$, given below and represented in Fig. 4.

$$T(x) = \begin{cases} \gamma x \left(1 - \frac{|x|}{S}\right)^P & |x| \le S \\ x & \text{elsewhere} \end{cases} \tag{15}$$

where x is the input signal, S the upper limit for nonlinear enhancement, γ the gain factor and P defining the rate of attenuation towards S.

Image features are emphasized thanks to better resolution and directional properties of the SPT. The contrast enhancement at each level and orientation is obtained by adapting the parameters γ and S to each subband.

The proposed method can be summarized in five steps:

– *Step 1*: Convert the original image f from rgb color space to Lab;
– *Step 2*: Use SPT to decompose the image luminance L into three levels and four orientations at each level as shown in Fig. 3;

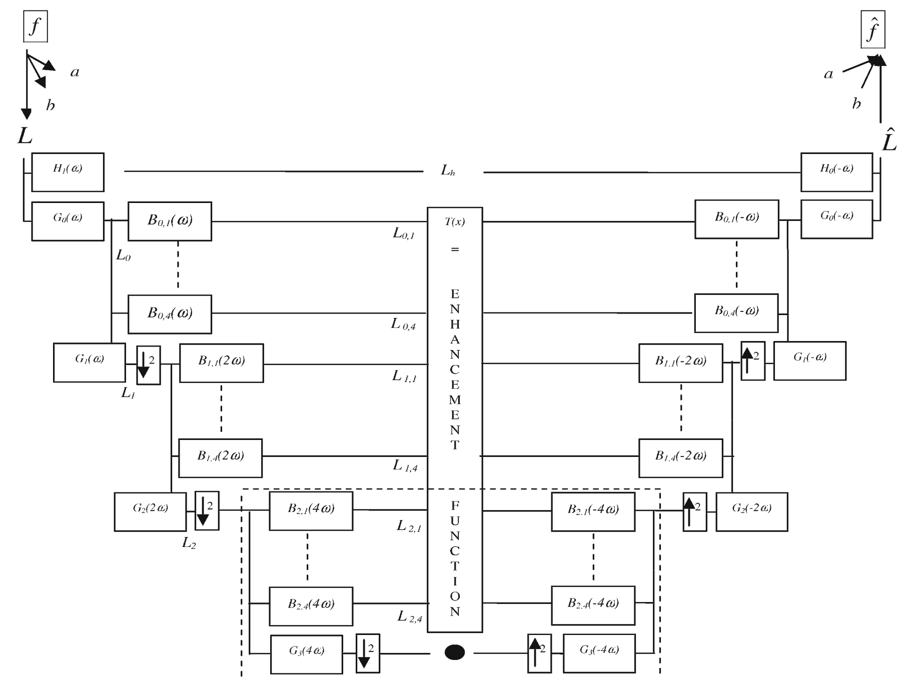

Fig. 3 The functioning diagram of the proposed method (for three levels of decomposition)

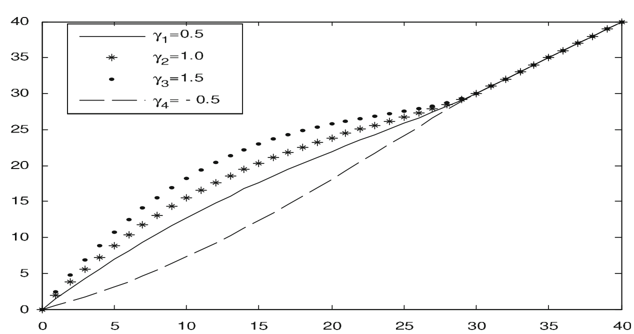

Fig. 4 Enhancement function according to Eq. (15) for $S = 30$, $P = 1.5$, and various values of γ

– *Step 3*: Use a nonlinear function with adaptive gain factor γ at each level to enhance those oriented band-pass components only;
– *Step 4*: Reverse pyramid decomposition process for reconstruction. Using the oriented and enhanced band-pass sub-images to get at the end the enhanced luminance image $\hat{L}$;
– *Step 5*: Convert enhanced $\hat{L}ab$ image back to enhanced $\widehat{rgb}$ color space.

4 Contrast enhancement evaluation

The assessment of image enhancement is rather a difficult task. Generally contrast enhancement is evaluated subjectively in terms of details visibility, sharpness, colour appearance and many other perceptual features. In many applications image enhancement could be also evaluated with regard to the quality of the final output at higher level tasks. There are only a few ad hoc objective measures for image enhancement evaluation [18]. The proposed contrast enhancement method is objectively evaluated using a spectral energy analysis [33] and a multi-resolution visibility map based on the perceptual filter introduced in [34].

4.1 Energy spectral analysis

The proposed method is based on a directional and band-limited analysis which allows the evaluation of energy variation in each sub-band and orientation. Following the idea developed in [33], radial and angular spectrum energy are calculated before and after the contrast enhancement. These quantities are computed by analyzing the Fourier transform of the image before and after processing.

Let $F(u, v)$ be the centered discrete Fourier transform of the image $f(x, y)$ defined by:

$$F(u,v) = \frac{1}{XY}\sum_{x=0}^{X-1}\sum_{y=0}^{Y-1} f(x,y)(-1)^{x+y} \times \exp\left(-2j\pi\left(\frac{ux}{X}+\frac{vy}{Y}\right)\right) \quad (16)$$

where X and Y are the image size and (u, v) the spatial frequencies.

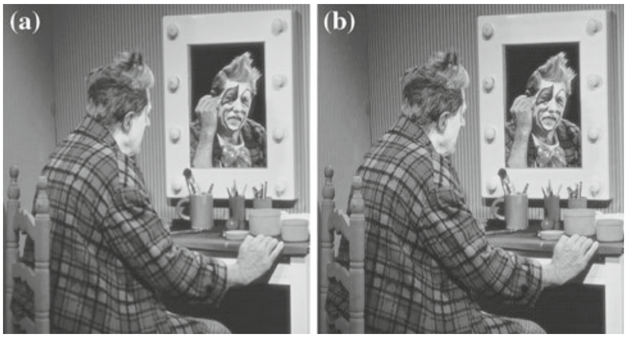

Fig. 5 Results of luminance enhancement. **a** Original image, **b** enhanced images with three levels and two directions with $\gamma = 3, 2, 1$ for the first three levels, respectively

The energy spectrum and phase spectrum are given by

$$|F(u, v)| = \sqrt{R^2(u, v) + I^2(u, v)} \tag{17}$$

$$\phi(u, v) = \tan^{-1}\left(\frac{I(u, v)}{R(u, v)}\right) \tag{18}$$

where $R(u, v)$ and $I(u, v)$ are the real and imaginary parts of $F(u, v)$, respectively.

Expressed in polar coordinates, the radial and angular energy spectrum can be calculated using Eq. (16), with $\omega = \sqrt{u^2 + v^2}$ being the radial frequency and θ is the angular frequency. Thanks to the symmetry of Fourier transform for $f(x, y) \geq 0$, the analysis is restricted to the angular interval $[0, \pi]$. The radial frequency ranges from 0 to $\omega_{\max}$, with max being the maximum. For a given radial frequency ω the average radial energy spectrum of the image before and after enhancement $E(\omega)$ and $E_e(\omega)$ are computed as follows:

$$E(\omega) = \frac{1}{M}\sum_{m=1}^{M} |F(\omega, \theta_m)| \quad \text{where} \quad \theta_m = \frac{m\pi}{M} \tag{19}$$

$$E_e(\omega) = \frac{1}{M}\sum_{m=1}^{M} |F_e(\omega, \theta_m)| \tag{20}$$

Where $F(\omega, \theta_m)$, $F_e(\omega, \theta_m)$ refer to Fourier spectrum in polar coordinates domain before and after enhancement and M is the angular sampling rate, i.e. the number of orientations.

Similarly, for a fixed analysis direction θ, the average angular energy spectrum is computed before and after enhanced using the following expression.

$$E(\theta) = \frac{1}{N}\sum_{i=0}^{N} |F(\omega_i, \theta)| \quad \text{where} \quad \omega_i = \frac{i\omega_{\max}}{N} \tag{21}$$

$$E_e(\theta) = \frac{1}{N}\sum_{i=0}^{N} |F_e(\omega_i, \theta)| \tag{22}$$

where N is the radial frequency sampling rate. This implementation is based on the assumption that the HVS demonstrates some selectivity properties to different frequency bands as discussed in [40]. Note that these quantities could be also used for selecting dominating directions in the image.

The curves shown in Fig. 6a and b corresponding to the original and enhanced luminance component Fig. 5a and b

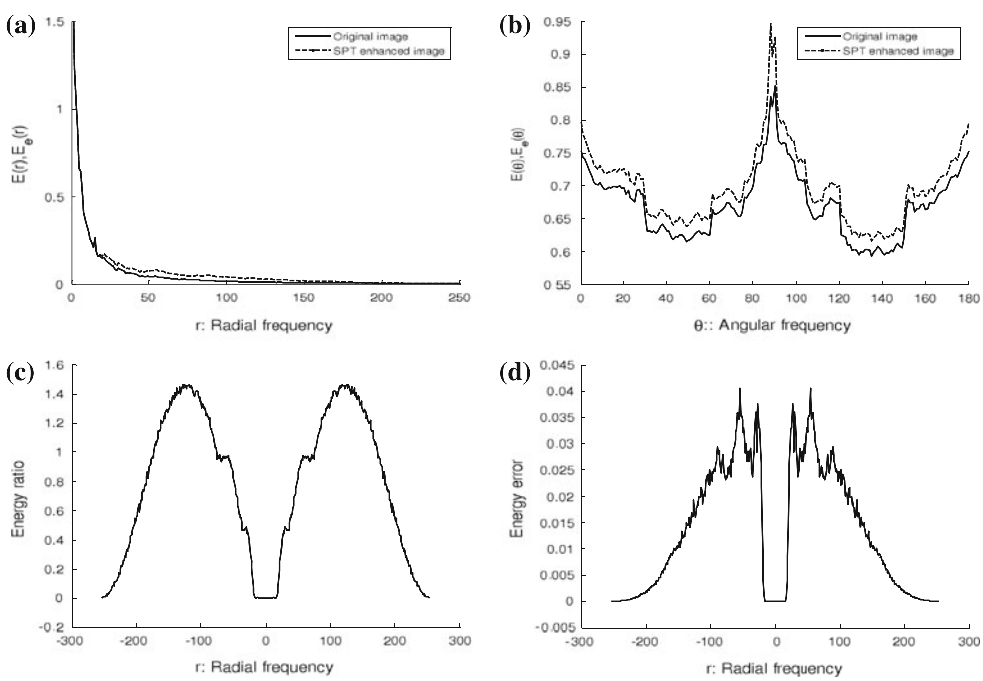

Fig. 6 Evaluation of the contrast enhancement for the image shown in Fig. 5: **a** radial frequency spectrum, **b** angular frequency spectrum, **c** energy ratio $\Delta(E)/E$ and **d** energy error $\Delta(E)$

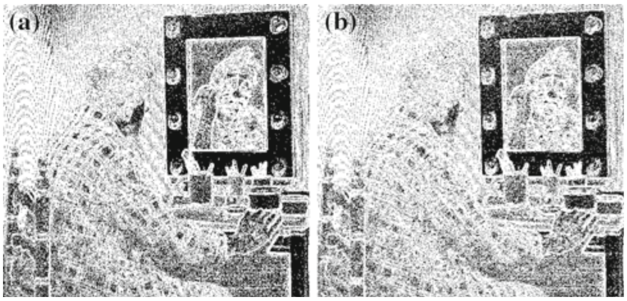

Fig. 7 The luminance visibility map before (**a**) and after enhancement (**b**)

clearly point out the selectivity characteristic of the proposed enhancement method. The energy ratio (ER) and the energy error (EE) curves Fig. 6c and d also clearly show the contrast enhancement effect on only the selected frequency bands. These results can be even more apparent in the map visibility which is discussed in the next section.

4.2 Visibility map analysis

In order to quantify and to visualize the effect of contrast enhancement on subtle details, a visibility map [34] is computed as follows:

$$V(i,j) = \begin{cases} 1 & C(i,j) \geq \mathrm{JNC} \\ 0 & C(i,j) < \mathrm{JNC} \end{cases} \tag{23}$$

where JNC is the Just-Noticeable Contrast and $C(i,j)$ is the local contrast.

This map is based on the local contrast defined as follows:

$$C(i,j) = \frac{|L(i,j) - L_s(i,j)|}{L_s(i,j)} \tag{24}$$

where $L(i,j)$ is the luminance of the pixel (i,j), and $L_s(i,j)$ is the immediate average surround luminance of its eight neighbors given by:

$$L_s(i,j) = \frac{1}{8} \sum_{k,l=-1,k,l\neq 0} L(i+k, j+l) \tag{25}$$

We use the Just-Noticeable Contrast JNC as defined in [41] and adapted by Belkacem and Beghdadi in [42] as follows:

$$V(i,j) = \begin{cases} \frac{C_w}{L_s(i,j)} \left(A + \sqrt{L_a(i,j)}\right)^2 & L_a(i,j) \geq L_s(i,j) \\ \frac{C_w}{L_s(i,j)} \left(A + \sqrt{\frac{L_s^2(i,j)}{L_a(i,j)}}\right)^2 & L_a(i,j) < L_s(i,j) \end{cases} \tag{26}$$

where C_ω is the Weber–Fechner JNC, $L_a(i,j)$ is the adaptation luminance and $A = 0.8$ is an experimentally measured parameter [41]:

$$L_a(i,j) = 0.923 L_s(i,j) + 0.771 L_g(i,j) \tag{27}$$

$L_g(i,j)$ is the global average luminance of the image f.

Figure 7 illustrates the luminance visibility maps of the image before and after enhancement with $C_w = 0.02$.

Fig. 8 Comparison of classical enhancement algorithm: the original image (**a**), unsharpening (**b**), histogram equalization (**c**), CLAHE (**d**), ELCE (**e**), steerable pyramid transform (**f**)

Fig. 9 Zoom comparison of classical enhancement algorithm: the original image (**a**), unsharpening (**b**), histogram equalization (**c**), CLAHE (**d**), ELCE (**e**), steerable pyramid transform (**f**)

5 Results and discussion

The proposed method has been tested on various color images and compared with some known contrast enhancement techniques, such as histogram equalization, Contrast-limited adaptive histogram equalization (CLAHE), Edge-based Local Contrast Enhancement (ELCE), unsharpening technique and two multiscale contrast enhancement methods (curvelet-based and MSRCR).

In the proposed method, the same mapping parameters are used for the whole sub-bands. Whereas, the gain is adapted at each decomposition level and for each sub-band. Here, we choose three levels of decomposition and four orientations $(0, \pi/4, \pi/2, 3\pi/4)$. Only the oriented band-pass components are enhanced by the nonlinear function. For each level, we use the optimum gain values $(\gamma_1 = 3, \gamma_2 = 2, \gamma_3 = 1)$. The parameter S controlling the range of the nonlinear enhancement is made to vary across the sub-bands and the level of decomposition. It is defined as $S = t.Mc$, where Mc is the maximum value of the coefficient at a given level of decomposition and sub-band and t is a factor $(0 < t <= 1)$. For example, if t is set to 1 all the band-pass components are enhanced.

The subjective quality of the obtained results is assessed in terms of visual appearance of the details, color preservation and noise sensitivity. Figures 8 and 9 illustrate the comparison of the proposed method with some known contrast enhancement methods. It could be noticed that, histogram-based methods produce significant color shift on many areas of the image as can be seen in Fig. 8c and d. The enhancement with ELCE tends to produce overshooting and other artefacts on textures (Fig. 8e). Unsharpening method tends to amplify noise and also produce overshooting (Fig. 8b). The differences are better visible on the clown hand (see the zoomed image in Fig. 9).

Figure 10 shows the results of applying multi-scale methods to color image [43]. The MSRCR (Fig. 10b) does not provide any significant contrast enhancement. It tends to gray out the image in many areas (see for example stairs, walls). This is mainly due to the averaging operation. Furthermore, the color restoration step in MSRCR used to compensate for the loss of saturation produce unpredictable results. In the curvelet-based method (Fig. 10c) the Luv representation is used instead of RGB. But all the curvelet coefficients of the three components Luv are processed. As a consequence, all the components are enhanced irrespective of their frequency content yielding thus a quasi-uniform contrast enhancement. It results in a loss of details visibility in some areas (see for example the wall) compared to image of Fig. 10d. In our method (Fig. 10d), only the mid-range frequency components are enhanced according to the band-pass nature of the HVS.

For the purpose of a full comparison evaluation, another color image is used. Figures 11, 12, and 13 display the original and the processed images with the classical methods, curvelet-based method, MSRCR and the proposed method. The objective evaluation is performed by using the energy spectrum and the visibility map. The obtained results are

Fig. 10 Comparison with multiscale enhancement methods: **a** the original image, **b** MSRCR method, **c** curvelet-based method, **d** the proposed method

displayed in Figs. 14 and 15. The limitations of the conventional methods are again clearly demonstrated through these results. To facilitate the visual comparison the visibility map associated to each processed image computed. Furthermore, a zone is selected and marked (blue circle) in the different images. It is shown that histogram-based methods (Fig. 11c and Fig. 12d) amplify noise and produce color saturation. The unsharpening method is also prone to noise amplification effect. On this example, the shortcomings of MSRCR method, such as graying and color shift, are clearly revealed in (Fig. 13b). On the other hand with SPT method (Figs. 12f, 13d), the enhancement is well balanced and controlled compared to curvelet-based method and MSRCR method. In the proposed method, only the medium or the desired details are made visible.

The objective evaluation of these results is illustrated in Figs. 14a–d and 15a–d, where the radial\angular frequency spectrum (RFS\AFS) before and after enhancement of the peppers image is visualized. The curves clearly show that the amplification of the energy is well localized. This is well observed in the angular frequency spectrum (AFS) curves of the enhanced image with SPT approach compared with the (AFS) of the original image and the other enhancement approach, as shown in Figs. 14b and 15.b. It is also observed that ELCE and unsharpening methods enhance uniformly the luminance image (i.e. all orientations from 0° to 180°). It

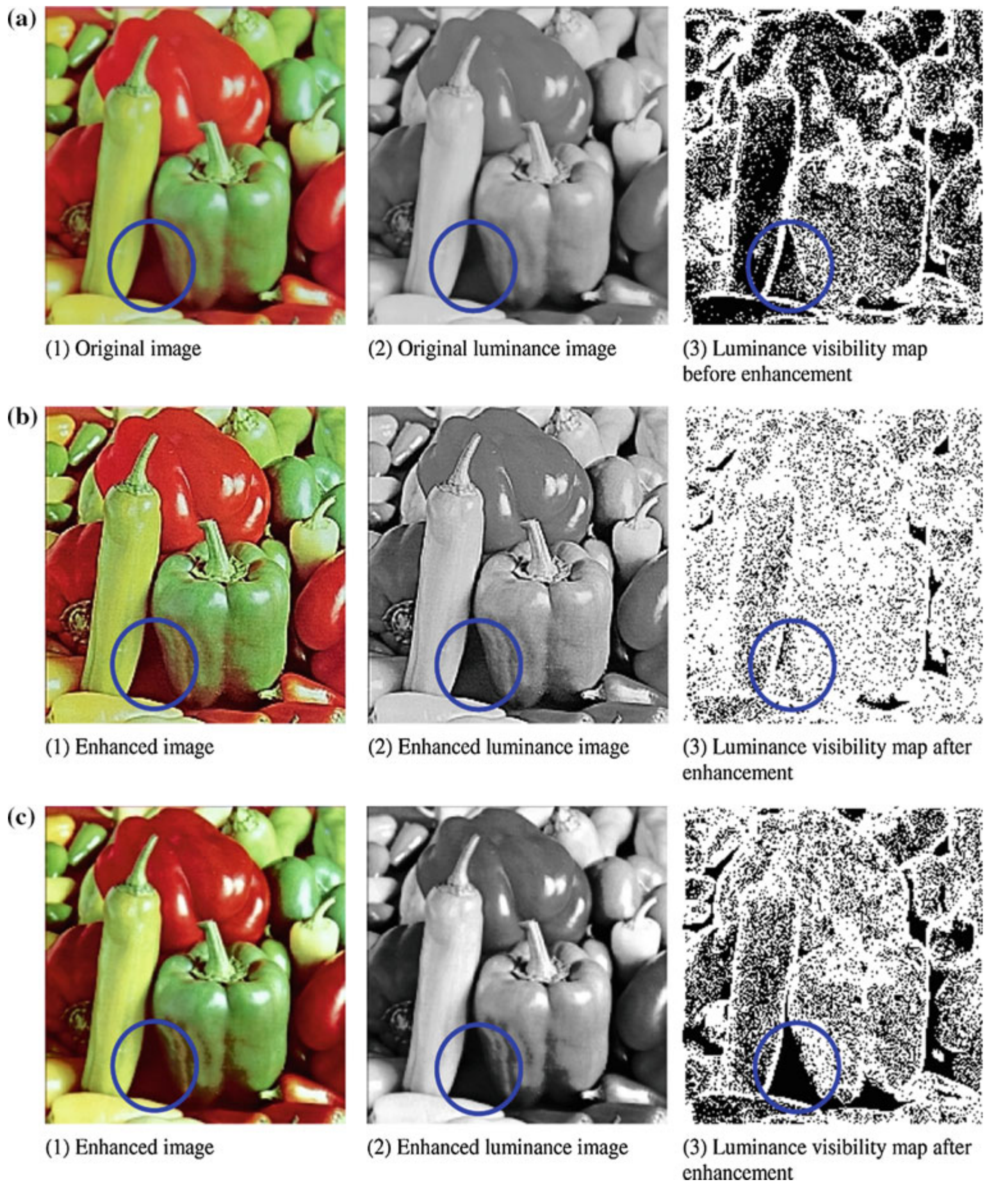

Fig. 11 Performance evaluation comparison: **a** original, **b** unsharpening, **c** histogram equalization (histeq)

could be also noticed that the histogram equalization tends to attenuate the energy of the image (see the AFS in Fig. 14b).

One can also notice that there are three parts in the Radial Frequency Spectrum (RFS) curves of the enhanced image. In the first and last parts, the spectrum remains unchanged as shown in Figs. 14a and 15a. This prevents from noise amplification in low band where it is more annoying then in the other bands. In the medium band, the spectrum of the enhanced image is increased and starts to attenuate in the last band. This allows us to bring out the invisible details in the medium frequency bands where the most important information is often masked.

To better show the improvement gained by our method, the energy ratio (ER) and the energy difference (ED) are computed from both the enhanced and the original luminance images (Figs. 14c, d, 15c, d) of the peppers image. So in our approach there are also three well distinguished parts. The low energy unchanged part, the increasing energy part in the medium frequency and the last one (high frequency band) where the energy gradually attenuates. In contrast, the energy curves of the other approaches show even a decrease in the first frequency band and higher energy in the other frequency bands (histogram-based methods). On the other hand ELCE approach presents an increase in the first frequency band

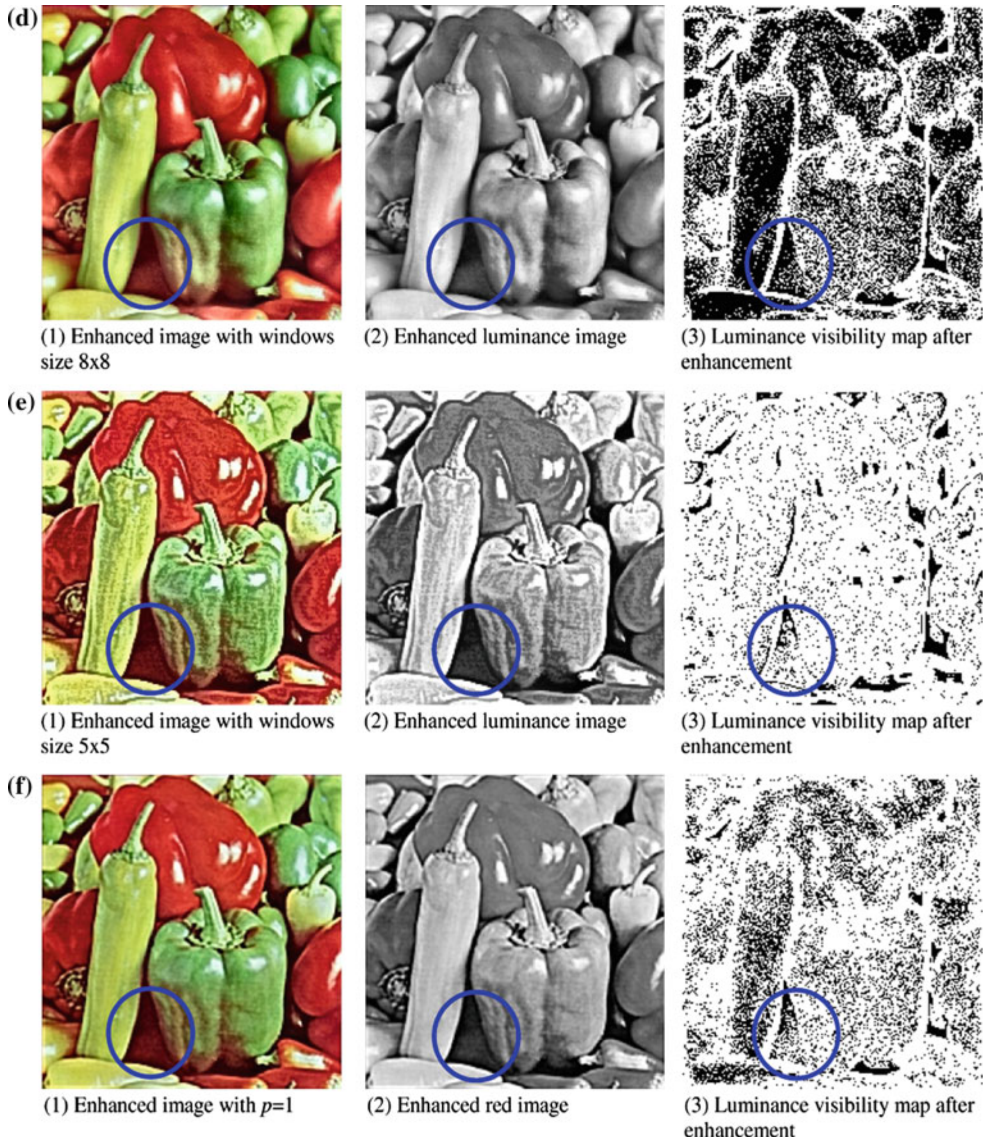

Fig. 12 Performance evaluation comparison (continued from Fig. 10): **d** contrast-limited adaptive histogram equalization (CLAHE), **e** edge-based local contrast enhancement (ELCE), **f** steerable pyramid transform (SPT)

followed with by the reverse phenomenon in the other frequency bands, which tends to amplify noise. The energy in the first frequency band of the MSRCR method is more increased followed by a decrease. Whereas, the curvelet-based method exhibits a reverse phenomena.

From the same test image (peppers image) a visibility map is computed before and after enhancement. We used the visibility map as a quality index of the enhanced image. A quality measure of enhancement could be derived from the visibility map. The blue circular zone in Figs. 11, 12, and 13 shows the progressive luminance visibility map of an object from the background before and after enhancement.

Notice that, applying the enhancement just to the band-pass components accentuates the visibility of details without increasing the noise in the low and high frequency and keeps the useful information in the reconstruction pyramid. It is worth to notice that the gain factor γ and the parameter S of the non-linear function have a great influence on the results.

These obtained results confirm that the use of a non-linear function and a pyramidal decomposition provides a controlled and selective contrast enhancement avoiding thus the artefacts encountered when using the other methods.

6 Conclusion and perspective

The frequency and directional selectivity of the HVS is exploited by using the steerable pyramid decomposition and

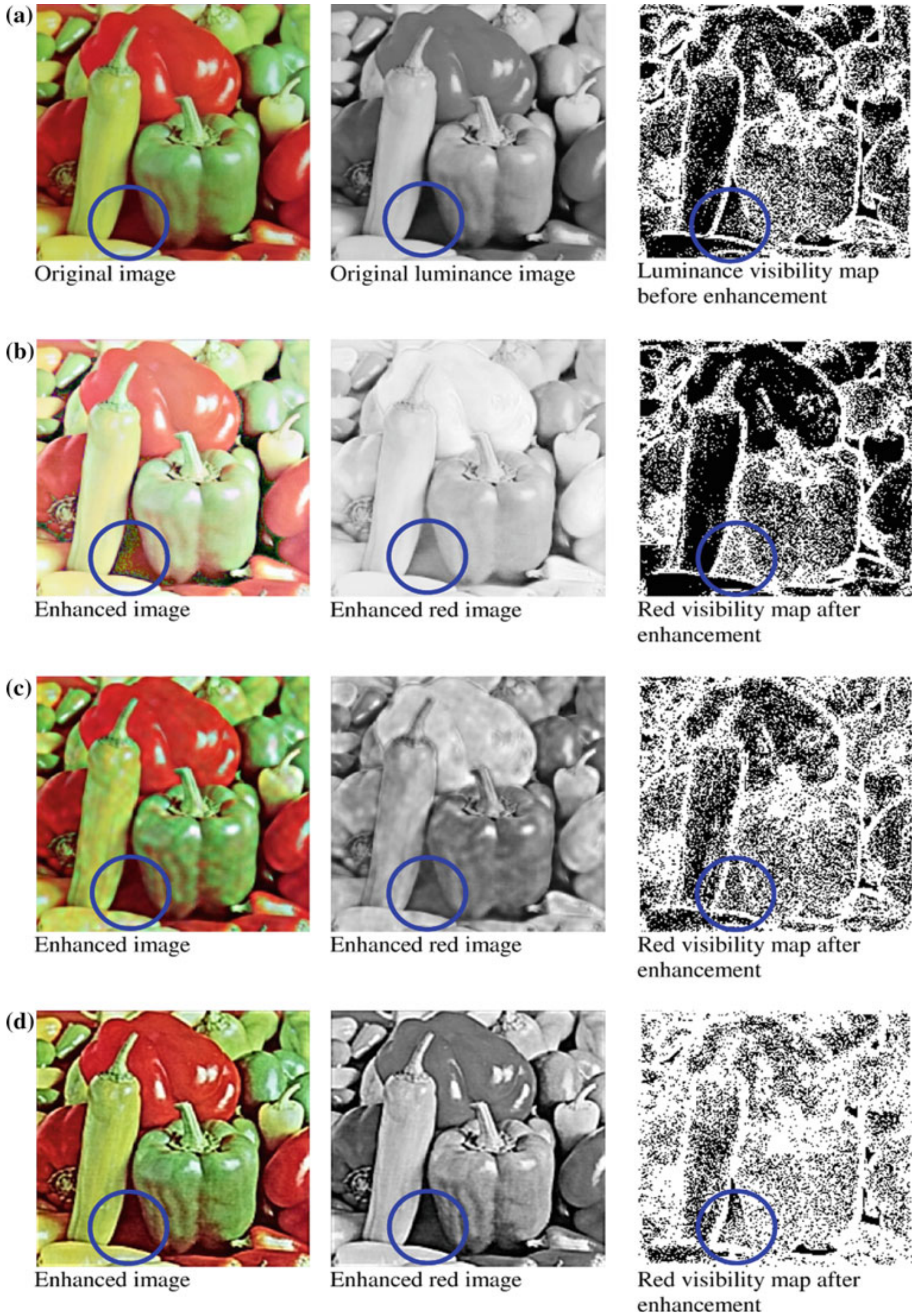

Fig. 13 Performance evaluation comparison (continued): **a** original, **b** MSRCR, **c** CUV, **d** SPT

reconstruction scheme, which is developed to give an efficient method for contrast enhancement. Furthermore, the proposed method gives more flexibility and better control for enhancing the visual quality of color images.

The method is evaluated both subjectively and objectively using a new contrast enhancement quality measure based on the frequency spectrum analysis, such as the AFS, RFS, ratio and energy difference. The proposed method has been also evaluated in terms of details visibility by analyzing the map visibility before and after processing the images.

According to the experiment results, the proposed method is superior to conventional methods and two new methods considered as the state-of-the-art in terms of perceptual image quality. The proposed method is efficient in enhancing subtle

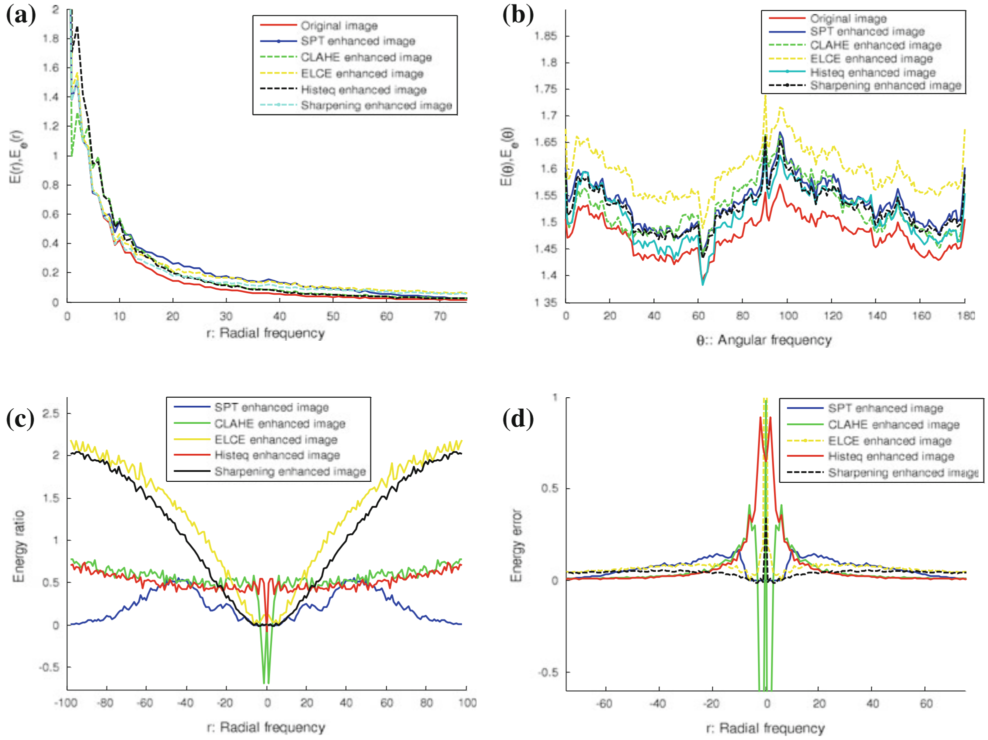

Fig. 14 Energy spectrum analysis: **a** radial frequency spectrum, **b** angular frequency spectrum, **c** energy ratio, **d** energy difference

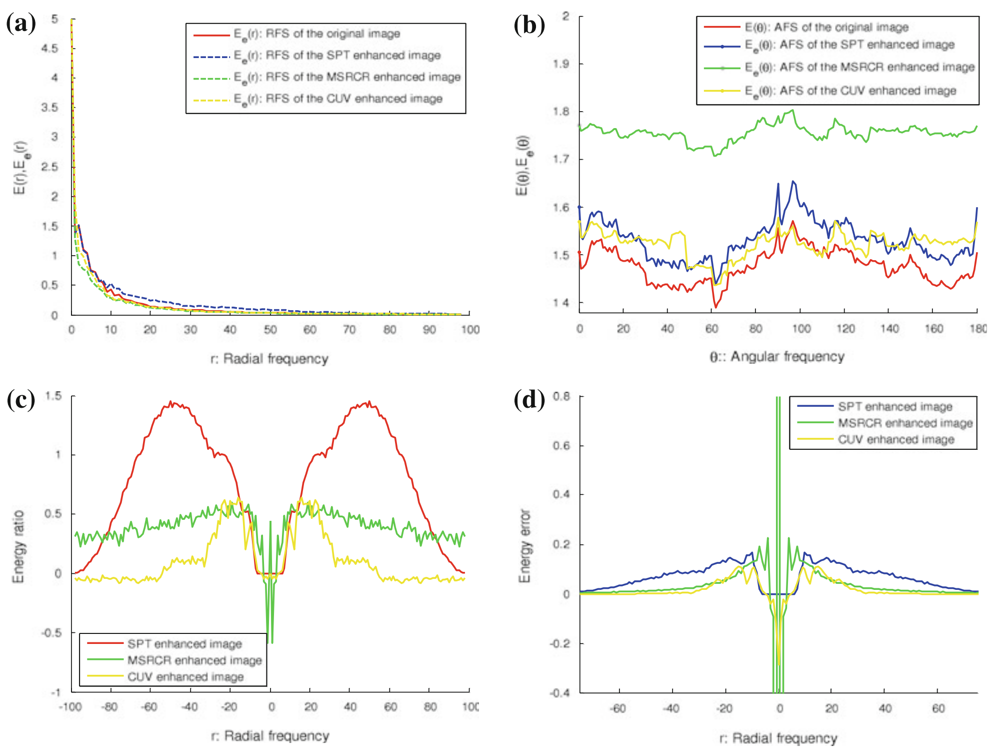

Fig. 15 Energy spectrum analysis continued: **a** radial frequency spectrum, **b** angular frequency spectrum , **c** energy ratio, **d** energy difference

details without amplifying noise. The use of directional and band-limited filters enables us to get enhanced images where the different structures are emphasized according to their orientation and position in the frequency domain. As perspectives we intend to pay specific attention to the non-linear function and to derive image enhancement index from the visibility map and the energy spectrum analysis.

Acknowledgments The authors would like to thank the editor and the three anonymous reviewers for their valuable comments and recommendations that result in significant improvement of the paper

References

1. Koschan, A., Abidi, M.: Digital Color Image Processing. Wiley Ed., New York (2008)
2. Buzuloiu, V., Ciuc, M., Rangayyan, R.M., Vertan, C.: Adaptive neighborhood histogram equalization of color images. Int. J. Electron. Image **10**(2), 445–450 (2001)
3. Trahanias, P.E., Venetsanopoulos, A.N.: Color image enhancement through 3-D histogram equalization. In: IEEE Proc. 11th IAPR. Joint Intl. Conf. Pattern Recognition, Hague, Netherlands, August 1992, pp. 545–548
4. Pitas, I., Kiniklis, P.: Multichannel techniques in color image enhancement and modeling. IEEE Trans. Image Proc. **5**, 168–171 (1996)
5. Niblack, W.: An Introduction to Digital Image Processing, 2nd edn. Prentice Hall, Englewood Cliffs (1986)
6. Dash, L., Chatterji, B.N.: Adaptive contrast enhancement and deenhancement. Pattern Recognit. **24**(4), 289–302 (1991)
7. Chatterji, B.N., Murthy, R.N.: Adaptive contrast enhancement for color images. In: IEEE Proc. ICICS. Joint Intl. Conf., Information, Communications and Signal Processing, Singapore, vol. 3, pp. 1537–1541, 9–12 September 1997
8. Strickland, R.N., Kim, C.S., McDonnell, W.F.: Digital color image enhancement based on the saturation component. Opt. Eng. **26**, 609–616 (1987)
9. Gupta, A., Chanda, B.: A hue preserving enhancement scheme for a class of color images. Pattern Recognit. Lett. **17**, 109–114 (1996)
10. Naik, S.K., Murthy, C.A.: Hue-preserving color image enhancement without gamut problem. IEEE Trans. Image Process. **12**(12), 1591–1598 (2003)
11. Toet, A.: Multiscale color image enhancement. Pattern Recognit. Lett. **13**(3), 167–174 (1992)
12. Laine, A.F., Fan, J., Yang, W.: Wavelets for contrast enhancement of digital mammography. IEEE Eng. Med. Biol. Mag. **14**, 536–550 (1995)
13. Huang, K., Wang, Q., Wu, Z.: Color image enhancement and evaluation algorithm based on human visual system. IEEE Proc. ICASSP, Joint Int'l. Conf., Acoustics, Speech, and Signal Processing, Montreal, Canada, May, 17-21, 2004, pp. 721–724
14. Xianghong, W., Shi-e, Y., Xinsheng, X.: An Effective Method to Colour Medical Image Enhancement. In: IEEE Proc. CME. Joint Int'l Conf., Complex Medical Engineering, Beijing, pp. 874–877, 23–27 May 2007
15. Xiao, D., Ohya, J.: contrast enhancement of color images based on wavelet transform and human visual system. In: Proceeding of the IASTED International Conference, pp. 58–63, 3–5 January 2007
16. Wu, Q., Schulze, M.A., Castleman, K.R.: Steerable pyramid filters for selective image enhancement application. In: IEEE ISCAS'98, Joint Int'l. Sym. on circuits and systeme, Monterey, California, vol. 5, pp. 325–328, May 31– June 3 1998
17. van den Branden Lambrecht, C.J. (ed.): Special issue on image and video quality metrics. Signal Process. **70** (3), 153–154 (1998)
18. Agaian, S.S., Panetta, k., Grigoryan, A.M.: Transform-based image enhancement algorithms with performance measure. IEEE Trans. Image Process. **10**(3), 367–382 (2001)
19. Land, E.H.: Recent advances in retinex theory and some implications for cortical computations: color vision and the natural image. Proc. Nat. Acad. Sci. USA **80**, 5163–5169 (1983)
20. Jobson, D.J., Rahman, Z., Woodell, G.A.: Properties and performance of a center/surround retinex. IEEE Trans. Image Process. **6**(3), 451–462 (1997)
21. Meylan, L., Süsstrunk, S.: High dynamic range image rendering with a Retinex-based adaptive filter. IEEE Trans. Image Process. **15**, 2820–2830 (2006)
22. Choi, D.H., Jang, I.H., Kim, M.H., Kim, N.C.: Color image enhancement based on single-scale retinex with a jnd-based nonlinear filter. In: IEEE Proc. ISCAS. Joint Int'l. Symposium Circuits and Systems, New Orleans, USA, pp. 3948–3951, 27–30 May 2007
23. Rahman, Z., Jobson, D., Woodell, G.A.: Multiscale retinex for color image enhancement. In: Proceedings of the IEEE International Conference on Image Processing, IEEE (1996)
24. Jobson, D.J., Rahman, Z., Woodell, G.A.: A multi-scale Retinex for bridging the gap between color images and the human observation of scenes. IEEE Transactions on Image Processing: Special Issue on Color Processing, vol. 6, pp. 965–976, July 1997
25. Wang, W., Zheng, J., Xian, S., Wang, J.: A fast multi-scale retinex algorithm for color image enhancement. In: IEEE proc., Int. Conf. on Wav. and Pattern Recognition, Hong Kong, pp. 80–85, 30–31 August 2008
26. Meylan, L., Alleysson, D., Süsstrunk, S.: A model of retinal local adaptation for the tone mapping of color filter array images. J. Opt. Soc. Am. A (JOSA A) **24**(9), 2807–2816 (2007)
27. Cherifi, D., Beghdadi, A., Belbachir, A.H.: A multiscale and multi-orientation contrast enhancement method for digital mammography. In: IEEE Proc. 3th ISCCSP, Joint Int'l. Sym. on com., control and signal proc., St Julians, Malta, pp. 312–315, 12–14 March 2008
28. Hummel, R.: Image enhancement by histogram transformation. Comput. Vis. Graph. Image Process. **6**(2), 184–195 (1977)
29. Reza, A.M.: Realization of the contrast limited adaptive histogram equalization (CLAHE) for real-time image enhancement. VLSI Signal Process **38**(1), 35–44 (2004)
30. Beghdadi, A., Le Negrate, A.: Contrast enhancement technique based on local detection of edges. Comput. Vis. Graph. Image Process. **46**, 162–174 (1989)
31. Alaya Cheikh, F., Khriji, L., Gabbouj, M.: Unsharp masking-based approach for color image processing. In: Proc. of the IX European Signal Processing Conference EUSIPCO-98, vol. 2, pp. 1033–1036, Island of Rhodes, Greece, 8–11 September 1998
32. Starck, J.L., Murtagh, F., Candes, E.J., Donoho, D.L.: Gray and color image enhancement using the curvelet transform. IEEE Trans. Image Process. **12**(6), 706–717 (2003)
33. Beghdadi, A., Deriche, M.: Features extraction from fingerprints using frequency domain analysis. In: IEEE Proc. Workshop On Signal Processing and its Applications, Brisbane, Australia, pp. 14–15, December 2000
34. Iordache, R., Beghdadi, A., Viaris de Lesegno, P.: Pyramidal perceptual filtering using Moon and Spencer contrast. In: The Int. Conf. on Image Processing ICIP'2001, Thessaloniki, Greece, October 2001
35. Freeman, W.T., Adelson, E.H.: The design and use of steerable filters. IEEE Trans. Pattern Anal. Mach. Intell. **13**, 891–906 (1991)
36. Simoncelli, E.P., Freeman, W.T., Adelson, E.H., Heeger, D.J.: Shiftable multiscale transform. IEEE Trans. Inform. Theory **38**(2), 587–607 (1992)

37. Karasaridis, A., Simoncelli, E.: A filter design technique for steerable pyramid image transforms. Proc. IEEE ICASSP **4**, 2387–2390 (1996)
38. Simoncelli, E.P., Freeman, W.T.: The steerable pyramid: a flexible architecture for multi-scale derivative computation. In: Second Int'l Conf on Image Proc, vol. 3, pp. 444–447, Washington, DC, October 1995
39. Burt, P.J., Adelson, E.H.: The Laplacian pyramid as a compact image code. IEEE Trans. Commun., vol. COMM-31, pp. 532–540, April 1983
40. Porat, M., Zeevi: The generalized Gabor scheme of image representation in biological and machine vision. IEEE Trans. Pattern Anal. Mach. Intell. **10**, 452–467 (1988)
41. Moon, P., Spencer, D.E.: The visual effect of nonuniform surrounds. J. Opt. Soc. Am. **35**, 233–248 (1945)
42. Belkacem-Boussaïd, K., Beghdadi, A.: A new image smoothing method based on a simple model of spatial processing in early stages of human vision. IEEE Trans. Image Process. **9**, 220–226 (2000)
43. http://www-stat.stanford.edu/~jstarck/contrast.html